Bioactive Materials 5 (2020) 1127–1137

Contents lists available at ScienceDirect

Bioactive Materials

journal homepage: http://www.keaipublishing.com/biomat

Reactive mesoporous silica nanoparticles loaded with limonene for improving physical and mental health of mice at simulated microgravity condition

Zhiguo Lu[a,c,1], Jianze Wang[a,1], Lina Qu[b], Guanghan Kan[b], Tianlu Zhang[a,c], Jie Shen[a,c], Yan Li[a], Jun Yang[a], Yunwei Niu[d,e], Zuobing Xiao[d,e], Yinghui Li[b,*], Xin Zhang[a,**]

[a] State Key Laboratory of Biochemical Engineering, Institute of Process Engineering, Chinese Academy of Sciences, Beijing, 100190, PR China
[b] State Key Laboratory of Space Medicine Fundamentals and Application, China Astronaut Research and Training Center, Beijing, 100094, China
[c] School of Chemical Engineering, University of Chinese Academy of Sciences, Beijing, 100049, PR China
[d] Shanghai Research Institute of Fragrance and Flavor Industry, Shanghai, 200232, PR China
[e] School of Perfume and Aroma Technology, Shanghai Institute of Technology, Shanghai, 200233, PR China

ARTICLE INFO

Keywords:
Reactive mesoporous silica nanoparticles
Slow release of limonene
Simulated microgravity condition
Improvement of physical health
Improvement of mental health

ABSTRACT

Astronauts are under high stress for a long time because of the microgravity condition, which leads to anxiety, affects their learning and memory abilities, and seriously impairs the health of astronauts. Aromatherapy can improve the physical and mental health of astronauts in a way that moisturizes them softly and silently. However, the strong volatility of fragrances and inconvenience of aroma treatment greatly limit their application in the field of spaceflight. In this study, reactive mesoporous silica nanoparticles were prepared to encapsulate and slowly release limonene. The limonene loaded nanoparticles were named limonene@mesoporous silica nanoparticles-cyanuric chloride (LE@MSNs-CYC). LE@MSNs-CYC were then applied to wallpaper to improve the convenience of aromatherapy. LE@MSNs-CYC could chemically react with the wallpaper, thus firmly adsorbed on the wallpaper. In the following, the mice were treated with hindlimb unloading (HU) to simulate a microgravity environment. The results showed that 28-day HU led to an increase in the level of anxiety and declines in learning, memory, and physical health in mice. LE@MSNs-CYC showed significant relief effects on anxiety, learning, memory, and physical health of HU treated mice. Subsequently, the molecular mechanisms were explored by hypothalamic-pituitary-adrenal axis related hormones, immune-related cytokines, learning, and memory-related neurotransmitters and proteins.

1. Introduction

Astronauts are in the compound environments of microgravity and airtight during the flight mission [1–4]. These environments seriously affect the physical and mental health of astronauts [5–8]. In particular, special work in high-stress environment, poor sleep conditions caused by microgravity environment, and loneliness caused by a confined habitat cause their psychological problems such as anxiety and decline of cognitive function [9–13]. Long term anxiety reduces the immune function of astronauts and further damages their health [14,15]. Besides, the decline in cognitive function decreases the efficiency of astronauts and further affects the space mission.

The traditional way to raise the level of astronauts' physical and mental health is to relax them through hearing, vision and touch, such as listening to music, watching movies, and playing video games [16]. However, these methods are all intentionally doing some things, which waste the time and energy of astronauts and make them tired. Besides, drug therapy can also improve the physical and mental health of astronauts. However, the drugs have side effects. In addition, astronauts are not easy about mentally accepting medication.

Fragrances have the function of regulating the central nervous system and aromatherapy has been widely used in anti-anxiety and improving cognitive memory [17–20]. There is an ancient Chinese poem that on the heels of the wind it slips secretly into the night; silent

Peer review under responsibility of KeAi Communications Co., Ltd.
* Corresponding author.
** Corresponding author.
E-mail addresses: yinghuidd@vip.sina.com (Y. Li), xzhang@ipe.ac.cn (X. Zhang).
[1] These authors contributed equally to this work.

https://doi.org/10.1016/j.bioactmat.2020.07.006
Received 5 June 2020; Received in revised form 13 July 2020; Accepted 14 July 2020

and soft, it moistens everything. The aromatherapy is carried out in moistening things softly and silently. So, it does not consume the time and energy of astronauts and does not make the astronauts tired. However, most kinds of fragrances are highly volatile [21–24]. So, fragrant molecules are released into the air completely in a short time. The high and unstable concentration of fragrant molecules in the air seriously weakens the effect of aromatherapy on astronauts and may cause astronauts discomfort. Besides, fragrances need to be added to the daily necessities of astronauts for more convenient aromatherapy. Therefore, the keys to improving the effect of aromatherapy on astronauts are to slow down the release rate of fragrances and the firm adhesion of fragrances molecules on the daily necessities of astronauts.

With the developments of nanotechnology and material chemistry, many kinds of nanomaterials have been used to load and slow-release guest molecules. For example, nanomaterials such as liposomes or micelles can encapsulate the guest molecules and prevent the release of the guest molecules by their dense shells [25–28]. The cationic nanomaterials can adsorb anionic guest molecules through electrostatic interaction [29–31]. Many nanoparticles can form chemical bonds with guest molecules, thus loading and controlling the release of guest molecules [32–36]. However, most fragrant molecules are highly volatile, neutral, and lack of chemical groups that can form chemical bonds with nanomaterials. Therefore, the above nanomaterials are not suitable for the encapsulation of fragrant molecules. In contrast, mesoporous silica nanoparticles (MSNs) have strong adsorption capacity for volatile molecules due to their large specific surface area [37–39]. The adsorption phenomenon depends on the interaction between the adsorbent surface and the adsorbate. These effects mainly include chemical bonds, hydrogen bonds, hydrophobic bonds, and van der Waals forces [40]. Therefore, MSNs are suitable for encapsulation and slow release of fragrance molecules. Paper is the most commonly used material in the daily life of astronauts, such as books, notebooks, and wallpapers. Therefore, the paper is an ideal choice for the adhesion of fragrances.

In this study, reactive MSNs were designed and prepared to encapsulate limonene for the application to wallpaper. As shown in Fig. 1A, MSNs modified with a large number of amino groups were synthesized and named MSNs-NH_2. The MSNs-NH_2 formed covalent bonds with cyanuric chloride (CYC) to obtain CYC modified MSNs (MSNs-CYC). The MSNs-CYC physically adsorbed the fragrant molecules limonene into their mesoporous structures to obtain the limonene-loaded MSNs-CYC. Wallpaper is a fiber structure formed by macromolecular polysaccharides such as cellulose. Therefore, there are a lot of hydroxyl groups on the surface of the wallpaper. CYC is an important component of reactive dyes. It is mainly used to form a strong covalent connection with the amino groups or hydroxyl groups on the surface of the substrate, to avoid the dye falling off the substrate. Therefore, MSNs-CYC could form strong covalent bonds with wallpaper, which improve the adsorption capacity of the nano-fragrances and prevent them from falling off the wallpaper. As shown in Fig. 1B, mice were cultured at the simulated microgravity condition by hindlimb unloading (HU) with −30° angle [41]. The long and thin mesoporous structure of MSNs-CYC and their strong adsorption capacity for fragrance led to the slow release of limonene. The effects of slowly released limonene on improvement in physical health, anti-anxiety, and improvement of learning and memory of mice were evaluated. The mechanisms were explored by the measurements of hypothalamic–pituitary–adrenal (HPA) axis related hormones, immune-related cytokines, learning, and memory-related neurotransmitters and proteins.

2. Materials and methods

2.1. Materials

Limonene (95%), super dry tetrahydrofuran (THF, 99.5%), cyanuric chloride (CYC, 99%), (3-aminopropyl) triethoxysilane (APTES, 99.5%) were purchased from Energy Chemical. Hexadecyltrimethylammonium bromide (CTAB, 99%) and Tetraethylorthosilicate (TEOS, 98%) were purchased from J&K Scientific. N, N-diisopropylethylamine (DIPEA, 99%) was obtained from Tokyo Chemical Industry (TCI). Ammonium hydroxide (28%), dichloromethane (99%), acetone (99%), methanol

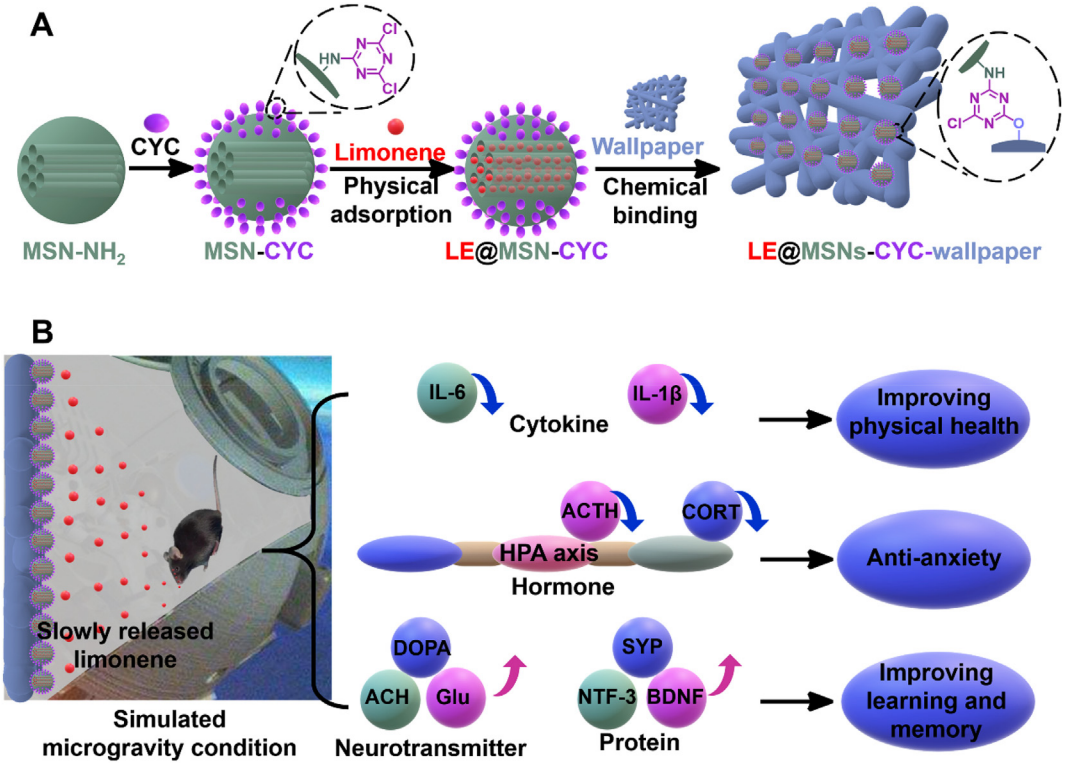

Fig. 1. (A) The schematic diagram of the preparation of MSNs-CYC, the encapsulation of limonene, and the application of limonene loaded MSNs-CYC to wallpaper. (B) The effects of slowly released limonene on anti-anxiety and improvement of learning and memory of the mice that cultured at simulated microgravity condition.

(99%), hydrochloric acid (HCl, 36.5%), and ethanol (99%) were purchased from Sinopharm Chemical Reagent CO., Lt.

2.2. Preparation of MSNs-CYC

CTAB (400 mg) was added into deionized water (140 mL) under the ultrasonic condition for 15 min. Ammonium hydroxide (3.5 mL) was then added into the solution under stirring for 30 min. When the solution was clear, TEOS (1.8 mL) and APTES (0.2 mL) were added rapidly into the surfactant sol under stirring for 2 h. The white precipitate was separated by filtration, washed with ethanol, and dried under vacuum for 12 h 1 g of the product was then re-dispersed into the mixture of ethanol and HCl (100 mL/1 mL, v/v) to extract CTAB. After refluxed three times at 80 ˚C for 24 h, the product was collected by centrifugation (4000 rpm) and extensively washed with deionized water and ethanol, which was denoted as MSNs-NH_2 [42].

Finally, the MSNs-NH_2 (100 mg) and cyanuric chloride (500 mg) were dissolved in THF (10 mL) under the sonicated condition for 10 min. DIPEA (500 μL) was then added into the solution under stirring at 0 ˚C. After 12 h, the product was collected by centrifugation (4000 rpm), washed with dichloromethane, acetone, methanol, and dichloromethane successively and dried under vacuum overnight, which was denoted as MSNs-CYC [43]. The modification of cyanuric chloride on the surface of MSNs was detected by Fourier transform infrared spectroscopy (FT-IR) and Raman spectra at 325 nm. The morphology of MSNs-CYC was observed by scanning electron microscopy (SEM) (JSM-6700F electron microscope) operating at an acceleration voltage of 10 kV and transmission electron microscopy (TEM) (JEM2100 electron microscope) operating at an acceleration voltage of 100 kV. The particle size distributions of MSNs-NH_2 and MSNs-CYC were measured by dynamic light scattering (DLS). The pore properties were detected via nitrogen adsorption-desorption isotherms. MSNs-CYC were heated at 180 ˚C to degas for 8 h. Then, the specific surface areas, pore size, and pore volume were measured and calculated by the Brunauer-Emmett-Teller (BET) method.

2.3. Preparation of LE@MSNs-CYC

Briefly, limonene (5 mL) was added into ethanol (10 mL) under the ultrasonic condition for 10 min. MSN-CYC (80 mg) was then added into the solution under vigorous stirring for 24 h. The content of limonene was measured by thermogravimetric analysis (TGA) [44].

2.4. Preparation of LE@MSNs-CYC treated wallpaper

The wallpaper (160 cm^2) was completely immersed in LE@MSNs-CYC solution under stirring at room temperature. After 24 h, the wallpaper was then dried at 50 ˚C for 2 h in an oven to obtain LE@MSNs-CYC treated wallpaper. The morphology of LE@MSNs-CYC-W was observed by SEM [45].

2.5. Measurement of the release of limonene

LE@MSNs-CYC (2 mL) were put in a dialysis bag (MWCO 3500) and incubated in deionized water (100 mL) at room temperature under horizontal shaking (200 rpm). At predetermined time intervals, deionized water (0.5 mL) was removed and the same volume of fresh solution was added. The quantification of the limonene was assessed using a gas chromatographer (GC) equipped with an HP-5 capillary column (30 m × 0.32 mm, 0.25 μm). The oven temperature program was initially set at 60 ˚C then raised to 150 ˚C at a heating rate of 20 ˚C/min. The flow rate of the carrier gas was 1 mL/min and the injector temperatures were set at 250 ˚C.

The release rate calculation formula is as follows:

$$\text{release rate}(\%) = W1/W2 \times 100\%$$

Where W_1 was the weight of limonene in ultrapure water, W_2 was the weight of total limonene in the NPs.

2.6. Animals

Female C57 mice (10 weeks) were purchased from the Academy of Military Medical Sciences of China. All procedures involving experimental animals were performed in accordance with protocols approved by the Committee for Animal Research of Peking University, China.

2.7. HU treatment

The HU treatment was performed by tail suspension according to the previous works of our laboratory [41,46]. Briefly, a 26 cm × 26 cm × 30 cm ground glass box with a crossbar was used for tail suspension. Two-thirds of the proximal tails were laterally bonded with adhesive sponge tape strips. The longitudinal strips were then fixed to the tail by medical tape strips wound circumferentially along the length of the tail. The mice were suspended by a small chain on the crossbar at the top of the cage. While the forelimbs remained in contact with the bottom of the cage, the length of the chain was adjusted as necessary to prevent the hind limbs of mice from touching any supportive surface. These animals were maintained at a 30˚ head-down tilt. LE@MSNs-CYC treated wallpaper, free limonene treated wallpaper, and untreated wallpaper were pasted on the ground glasses of glass box, respectively. The normal animals were maintained in the same environment as the HU treated mice, but without tail suspension and wallpaper.

2.8. Elevated plus-maze test

The elevated plus-maze consisted of two open arms and two closed arms, 10 × 50 (length × width) and the two arms of each type were opposite to each other. The maze was elevated 50 cm above the ground. The mice were then placed individually in the elevated plus-maze. The following parameters were automatically recorded by a video camera for 5 min: distance traveled in all the maze and the open arms of the maze [47].

2.9. Light-dark transition test

The apparatus for the light-dark transition test consisted of a cage divided into two chambers of equal size by a partition with a tunnel that allowed passage from one compartment to the other. One chamber is brightly illuminated by white diodes, whereas the other chamber is dark. The mouse was placed in the center of the light area with its back to the opening. The following parameters were automatically recorded by a video camera for 5 min: 1) Trajectory and the total distance of mice. 2) The movement distance of mice in the illuminated part of the cage. 3)The number of times the mouse entered the illuminated part of the cage [48].

2.10. Novel object recognition test

The novel object recognition test is a learning and a memory test method based on the principle that animals have a congenital tendency to explore new objects. In the habituation phase, the mouse was placed into individual square wooden boxes (60 cm × 60 cm × 60 cm) containing the same two objects for 5 min, and returned quickly to its housing cage. After 24 h, the mice were placed into the arena containing two different objects, one of which was replaced with a new object that differed in shape, color, and texture. Animals were allowed 5 min to explore. The following parameters were automatically recorded by a video camera: 1) Trajectory and the total distance of mice. 2) The times of exploration of the two objects. 3) The movement distance of mice to explore novel objects [49].

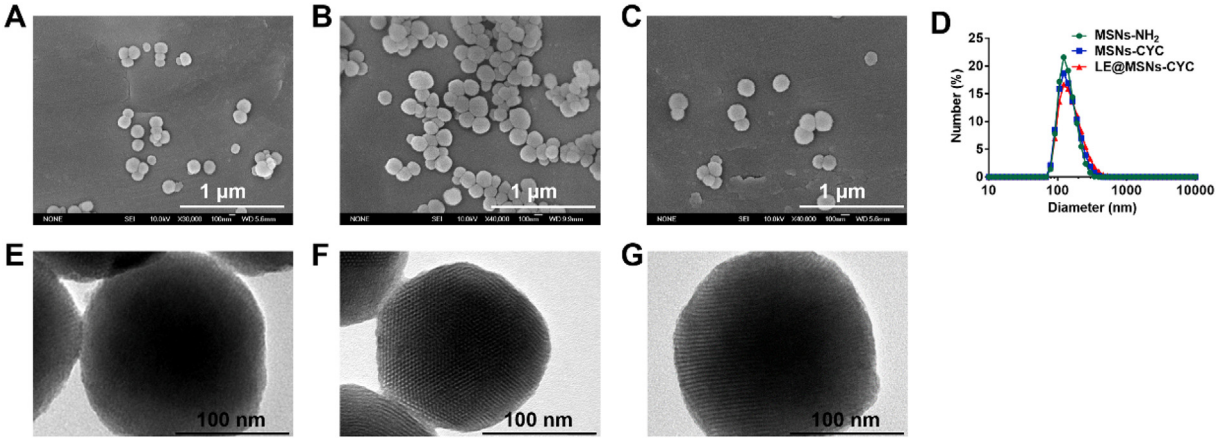

Fig. 2. (A–C) The SEM images of (A) MSNs-NH2 with CTAB, (B) MSNs-NH2 without CTAB and (C) MSNs-CYC. (D) The diameters of MSNs-NH2, MSNs-CYC, and LE@MSNs-CYC by DLS. (E–G) The TEM images of (E) MSNs-NH2 with CTAB, (F) MSNs-NH2 without CTAB, and (G) MSNs-CYC.

2.11. Morris water maze test

The experimental training period was 4 days and the mice were trained 4 times each day. The method of the experimental training stage is as follows. The mice were placed individually into the pool from four quadrants. The time that the mice reached the platform from the water and standing on it was recorded as the latency time. After finding the platform, the mice were allowed to stand on the platform for 10 s. If the rats stayed in the water for more than 90 s, they were gently dragged out of the water onto the platform and held there for 10 s before the next training. After the training, the platform was removed. The mice were placed individually in the pool facing the pool wall. The ratio of the time in the original quadrant of the total time was recorded, and the number of times that the rat crossed the original platform in 90 s was measured [50].

2.12. The measurement of neurotransmitters, corticosteroids and

The content of dopamine (DOPA), acetylcholine (ACH) glutamic acid (Glu), and γ-aminobutyric acid (GABA) in the brain were detected as representative neurotransmitters by liquid chromatography-mass spectrometry (LC-MS). The processing method and testing conditions referred to the previous work of our laboratory [51]. The expression level of cortisol and corticosterone in serum was also detected by LC-MS. Briefly, ether (500 μL) was added into serum samples (800 μL) and whirled for 5 min. The upper organic phase was collected by centrifugation (10000 rpm) and then repeat the above steps once. The products were blown dry with nitrogen and then dissolved by methanol (200 μL), fully whirled for 3 min and centrifuged at 10000 r/min for 10 min 100 μL of supernatant was taken to test by LC-MS.

2.13. Measurement of adrenocorticotropic hormone (ATCH), IL-6 and IL-β

The levels of ATCH, IL-6, and IL-β in the serum were detected by using the ELISA kit according to the manufacturer's protocols. Briefly, the serum samples were added to a 96-well ELISA plate and then reacted with relevant primary antibodies and horseradish peroxidase-labeled streptavidin. 3,3′,5,5′-Tetramethylbenzidine (TMB) was used as the substrate, and the absorbance was measured by a microplate reader.

2.14. Western blot analysis

The expression of synaptophysin (SYP), brain-derived neurotrophic factor (BDNF) and neurotrophic factor-3 (NTF-3) were measured by the Western blot. Briefly, The protein was separated by 10% SDS-PAGE and transferred to a nitrocellulose membrane (Millipore, USA). The membrane was then blocked with 5% skimmed milk in PBST and then incubated with primary antibody anti-SYP (1:10000), anti-BDNF (1:5000), anti-NTF-3 (1:2000), and anti-GAPDH (1:20000), respectively. The blots were washed five times in TBST before incubation with the appropriate secondary antibody and then visualized by ECL chemiluminescene Kit (Millipore, USA). The grey intensity of the western-blot bands was quantitatively analyzed by ImageQuant software.

2.15. Statistical analysis

All data were expressed as mean ± SD unless otherwise indicated. Statistical significance was analyzed using one-way ANOVA. Statistical differences in behavioral data were determined using two-way repeated measure ANOVA.

3. Results and discussion

3.1. Preparation and characterization of LE@MSNs-CYC treated wallpaper

The MSNs with amino groups were prepared by a sol-gel method to modify CYC and the template CTAB was removed by extraction. The MSNs-CYC were then synthesized by a substitution reaction of MSNs-NH_2 with CYC. As shown in Fig. 2A-C, there was no difference in morphology and size between MSNs-NH_2 before CTAB removal, MSNs-NH_2 after CTAB removal and MSNs-CYC. All of them were spherical and the diameters were about 160 nm. The distribution statistics of particle size was measured by dynamic light scattering (DLS). As shown in Fig. 7D, the diameters of MSNs-NH_2, MSNs-CYC, and LE@MSNs-CYC were 122.4, 132.5, and 141.8 nm, respectively. Subsequently, the internal structures of silica nanoparticles were observed by TEM. As shown in Fig. 2E, there were unclear pore structures only at the edge of nanoparticles. This is due to the large amount of CTAB in the pores of silica nanoparticles. After removing CTAB, the clear pore structure of MSNs-NH_2 was observed (Fig. 2F). The MSNs-CYC were shown in Fig. 2G. After the modification of CYC, the morphology of nanoparticles did not change significantly. This is because that CYC was a small molecule that was difficult to be observed by TEM.

The chemical groups of MSNs-NH_2 and MSNs-CYC were detected by FT-IR (Fig. 3A). For the FT-IR spectrum of CYC, the adsorption peak at 1512.9 cm^{-1} was assigned to the cyanuric ring vibrations. The FT-IR spectrum of MSNs-NH_2 presented the O–H, Si–O–Si stretching vibrations, and the N–H deformation vibrations of primary amine at 3402.6, 1100.8 and 1598.3 cm^{-1}. As shown in the FT-IR spectrum of MSNs-CYC, the adsorption peaks at 1516.6 and 1565.2 cm^{-1} were ascribed to the cyanuric ring vibrations and N–H deformation vibrations of secondary amine. These results proved that CYC was modified on silica

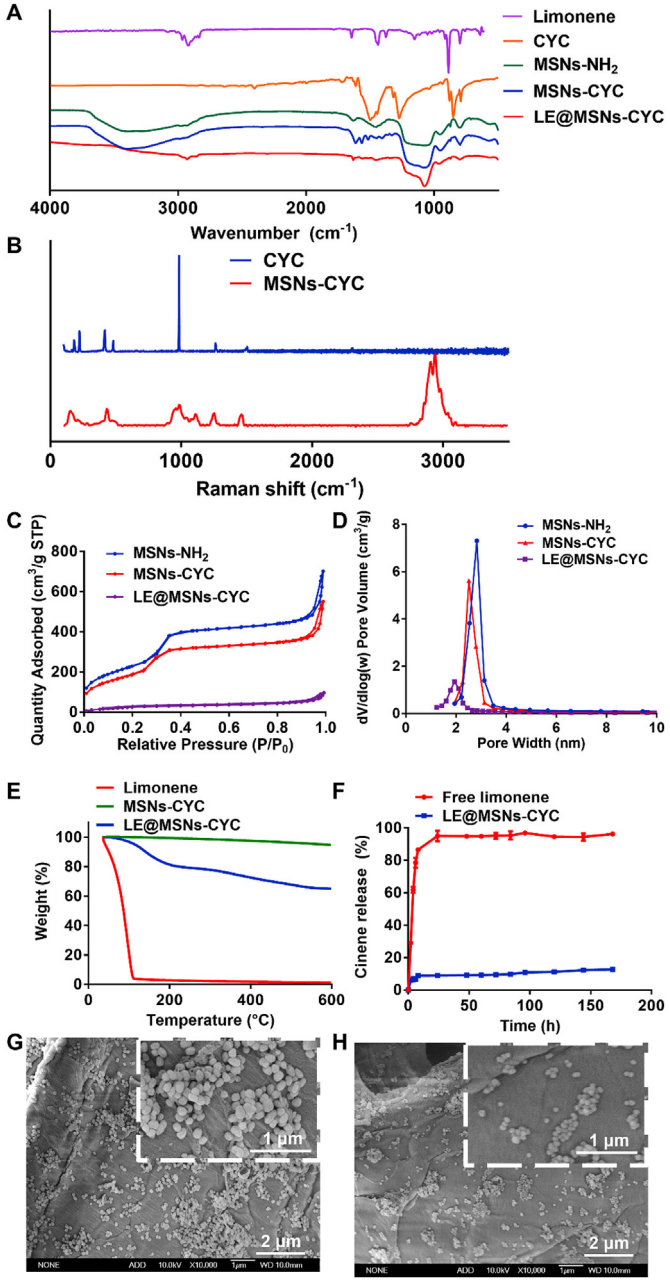

Fig. 3. (A) The FT-IR spectra of limonene, CYC, MSNs-NH2, MSNs-CYC, and LE@MSNs-CYC. (B) The Raman shifts of CYC and MSNs-NH2, MSNs-CYC, and LE@MSNs-CYC. (C) The N2 adsorption-desorption isotherm at 77 K for MSNs-NH2, MSNs-CYC, and LE@MSNs-CYC. (D) The pore diameter distribution of MSNs-CYC. (E) The TGA curves of limonene, MSNs-CYC, and LE@MSNs-CYC. Mean ± SD was shown (n = 3). (F) The release profiles of free limonene and LE@MSNs-CYC. (G) The SEM image of LE@MSNs-CYC treated wallpaper. (H) The SEM image of LE@MSNs-NH2 treated wallpaper.

nanoparticles. The chemical structure of MSNs-CYC was also detected by Raman spectra. As shown in Fig. 3B, the adsorption peak at 983.3 cm^{-1} was ascribed to the triazine ring of CYC. The adsorption peak at 432.8 cm^{-1} was assigned to the C–Cl vibration of CYC. The adsorption peak of 1465.6 cm^{-1} was attributed to the C═N vibration of CYC. The adsorption peak of 1108.4 cm^{-1} was assigned to the new C–N deformation vibrations of secondary amine. These results also proved that CYC was modified on silica nanoparticles.

Subsequently, limonene was adsorbed into the mesoporous structure of MSNs-CYC. For the FT-IR of limonene (Fig. 3A), the 1647.1 cm^{-1} was ascribed to the C═C stretching. The 2863, 2933, and 2979 cm^{-1} were ascribed to the C–H stretching. In the FT-IR of LE@MSNs-CYC, the C═C stretching and C–H stretching of limonene were clearly observed. These results indicated that limonene was encapsulated into MSNs-CYC. The properties related to mesopores of MSNs-NH_2, MSNs-CYC, and LE@MSNs-CYC were detected by a method of N_2 adsorption-desorption isotherm (Fig. 3C). The pore diameter, specific surface area, and pore volume were calculated based on the N_2 adsorption-desorption isotherm. As shown in Fig. 3D, the pore diameters of MSNs-NH_2, MSNs-CYC, and LE@MSNs-CYC were about 4.83, 4.08, and 1.94 nm, respectively. After modifying CYC, the pore size of MSNs-CYC was slightly reduced. But after encapsulating limonene, the pore size of LE@MSNs-CYC was significantly reduced. The specific surface areas of the pore diameters of MSNs-NH_2, MSNs-CYC, and LE@MSNs-CYC were about 849.28, 701.63, and 120.03 m^2/g, respectively. The pore volumes of MSNs-NH_2, MSNs-CYC, and LE@MSNs-CYC were about 1.03, 0.81, and 0.13 cm^3/g, respectively. After encapsulating limonene, the specific surface area of LE@MSNs-CYC was only 17% of MSNs-CYC. The pore volume of LE@MSNs-CYC was only 16% of MSNs-CYC. These results indicated that Limonene was effectively encapsulated by MSNs-CYC.

The limonene loading efficiency of LE@MSNs-CYC was measured by a TGA method. As shown in Fig. 3E, the free limonene began to decompose at 37.3 °C and completely decomposed at 109.3 °C. By comparison, the decomposition of limonene in LE@MSNs-CYC was started at about 80 °C and completed at about 500 °C. These results showed that the thermal stability of limonene was improved after being encapsulated by MSNs-CYC. The loading efficiency of LE@MSNs-CYC was calculated as 29.82% according to the results of TGA. Several reports notified that the physical adsorption resulted in the poor encapsulation and the loading efficiencies were about 10% [52,53]. This was mainly because the drugs they encapsulated were solid. Therefore, these solid drugs must be dissolved in the solvent during the adsorption process. The solid drug would enter the MSNs together with the drugs, thereby reducing the loading efficiency. In contrast, limonene is liquid. Therefore, limonene did not need to be dissolved in the solvent during the adsorption process. In other words, only limonene was encapsulated into MSNs, thereby improving the loading efficiency. The releases of limonene were then detected. As shown in Fig. 3F, more than 85% of free limonene was released within 8 h. At 24 h, limonene was released completely. In contrast, less than 10% of the fragrance was released from LE@MSNs-CYC. At 168 h (7 days), only 12.7% of limonene was released. These results demonstrated that LE@MSNs-CYC had excellent properties of sustained releasing fragrance. It was precisely due to the narrow mesoporous structure and strong adsorption capacity of MSNs-CYC that provided excellent thermal stability and slow-release ability for encapsulated limonene.

In the following, the LE@MSNs-CYC were applied to wallpaper. As a comparison, LE@MSNs without CYC were also applied to the wallpaper. The wallpapers were characterized by SEM. As shown in Fig. 3G and H, more silica nanoparticles were adhered to the wallpaper after modifying CYC. That was to say, CYC could significantly improve the adhesion ability of silica nanoparticles on wallpaper.

The most critical scientific problem to be solved for the application of nano-fragrance on wallpaper was the firm adsorption of nanoparticles on wallpaper. This was essentially the interaction between wallpaper and nanoparticles. Chemical bonds were more powerful than physical adsorption. To evaluate the firmness of nanoparticle adsorption on the wallpaper, the wallpaper adhered by nanoparticles was soaked in deionized water under stirring and detected by SEM. As shown in Fig. 4A-C, almost no LE@MSNs-CYC fell off the wallpaper in six days. By contrast, LE@MSNs without CYC began to fall off the wallpaper on the second day and most of the LE@MSNs fell off the wallpaper on the fourth day (Fig. 4D-F). On the sixth day, there were almost no LE@MSNs on the wallpaper. These results indicated that the modification of CYC significantly improved the adhesion fastness of nanofragrance on wallpaper. This was because the silica nanoparticles

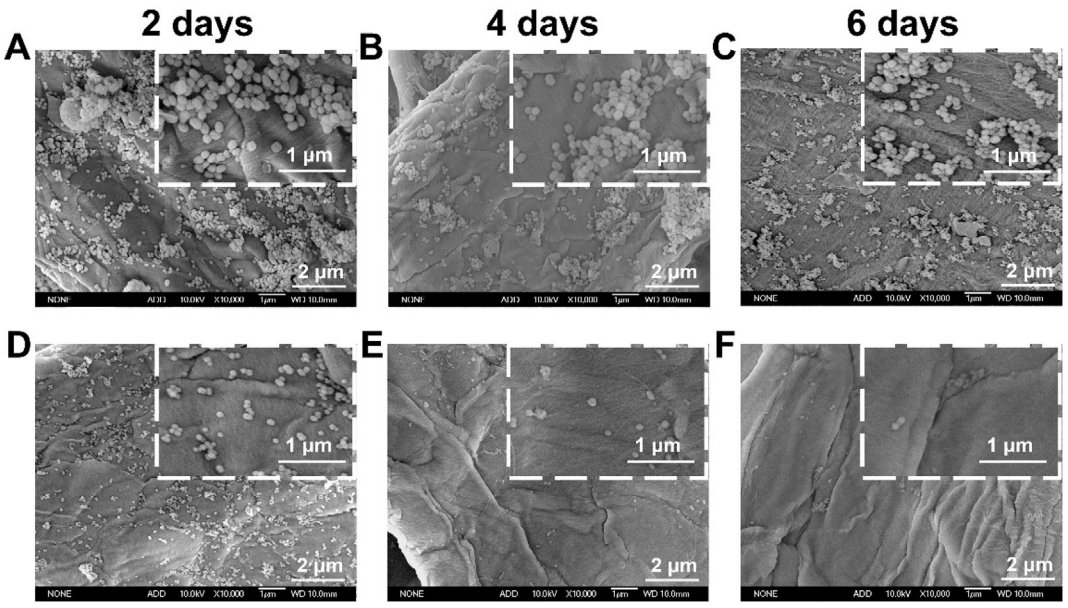

Fig. 4. (A–C) The SEM images of LE@MSNs-CYC treated wallpaper after soaked in deionized water under stirring for (A) 2 days, (B) 4 days, and (C) 6 days, respectively. (D–F) The SEM images of LE@MSNs treated wallpaper after soaked in deionized water under stirring for (D) 2 days, (E) 4 days, and (F) 6 days, respectively.

can chemically react with the wallpaper and form plenty of covalent bonds after modified with CYC. Therefore, LE@MSNs-CYC is a kind of reactive nanofragrance.

Although LE@MSNs-CYC were proven to hardly fall off the wallpaper, the biocompatibility of LE@MSNs-CYC treated wallpaper should be detected. Therefore, hematoxylin/eosin (HE) staining was performed to explicitly demonstrate the biocompatibility. As shown in Fig. 5, the major organs (heart, liver, spleen, lung, and kidney) were collected for HE staining. For LE@MSNs-CYC treated mice, free limonene treated mice, untreated mice, and normal mice, there were no obvious histopathological lesions. Therefore, LE@MSNs-CYC treated wallpaper had excellent biocompatibility.

3.2. The effects of LE@MSNs-CYC treated wallpaper on anti-anxiety of mice at simulated microgravity condition

The tails of mice were suspended to simulate a microgravity environment and the mice were maintained in a 30° head-down tilt. The mice were cultured with the fragrance treated wallpaper at the simulated microgravity condition for 28 days. Subsequently, the effects of LE@MSNs-CYC treated wallpaper on anti-anxiety of mice were evaluated by elevated plus-maze tests and light-dark transition tests.

The elevated plus-maze consists of a pair of open arms and a pair of closed arms that are higher from the ground. The open arms are in contact with the outside while the closed arms are isolated from the outside. Anxiety levels in mice can be assessed by recording and quantifying the movement distributions of mice in the open and closed arms. Briefly, mice have paradoxical feelings of fear and curiosity about their arms. The movement in the arm means that mice overcome fear and explore novelties. Therefore, the higher the proportion of movement in the open arms, the lower the level of anxiety in the mice [54,55]. The movements of mice in elevated plus-mazes were shown in Fig. 6A. Then, the total movement distances, movement distances in open arms, and percentages of movement distances in open arms were quantified. As shown in Fig. 6B-D, untreated mice had significantly less total movement distances, movement distances in open arms, and

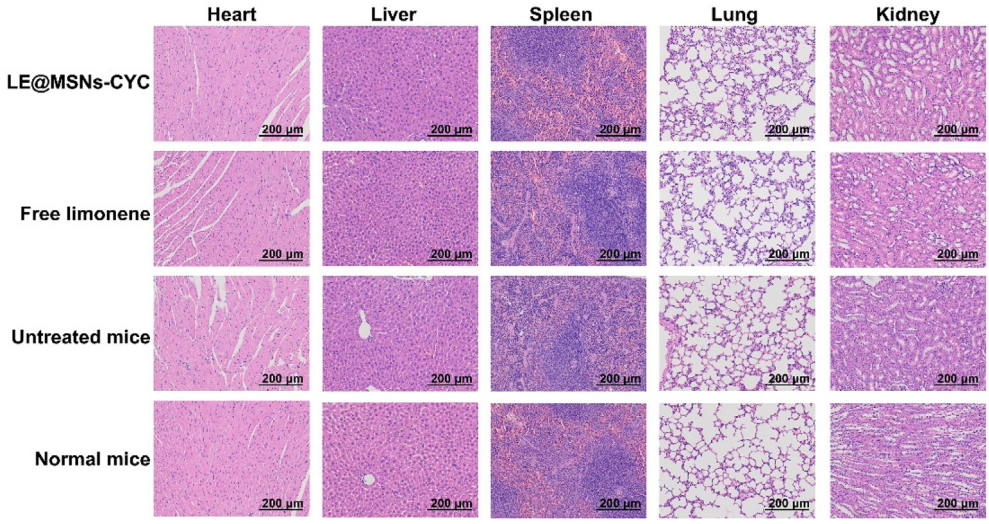

Fig. 5. HE staining of hearts, livers, spleens, lungs, kidneys. The scale bars were 200 μm.

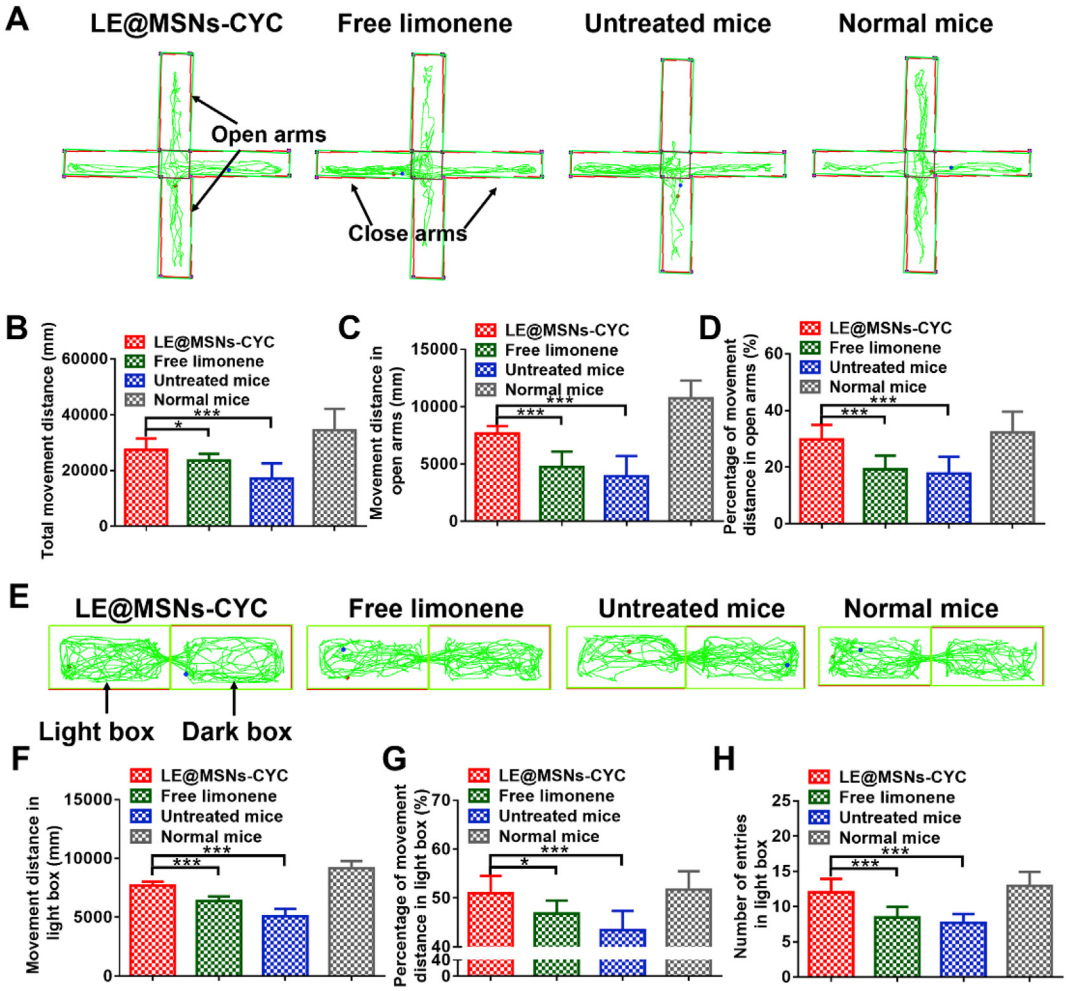

Fig. 6. (A) The movements of mice in the elevated plus-mazes. (B–D) The quantified results of Fig. 6A. (E) The movement of mice in light-dark transition tests. (F–H) The quantified results of Fig. 6E. Mean ± SD was shown (n = 12). *P < 0.05, **P < 0.01, ***P < 0.005.

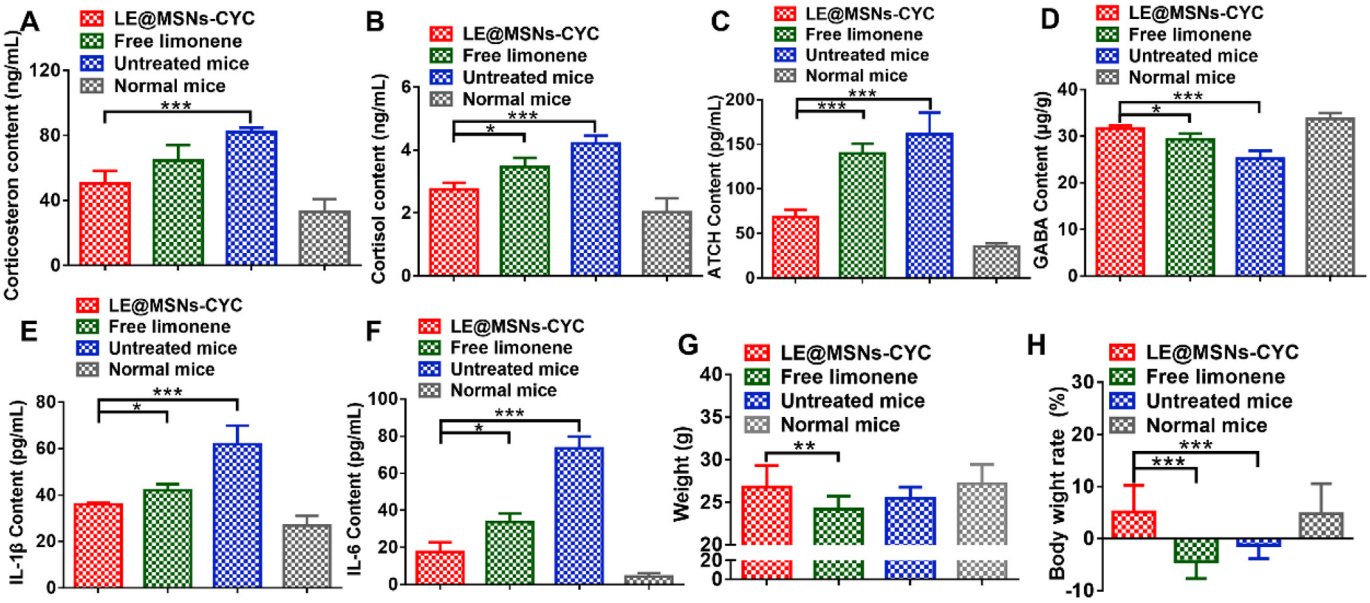

Fig. 7. (A) The content of corticosterone in the serum of mice. (B) The content of cortisol in the serum of mice. (C) The content of ATCH in the serum of mice. (D) The content of GABA in the brains of mice. (E) The content of IL-1β in the peritoneal macrophages of mice. (F) The content of IL-6 in the peritoneal macrophages of mice. (G) The body weights of mice after cultured for 28 days. (D) The body weight rate of mice after cultured for 28 days. Mean ± SD was shown (n = 3). *P < 0.05, **P < 0.01, ***P < 0.005.

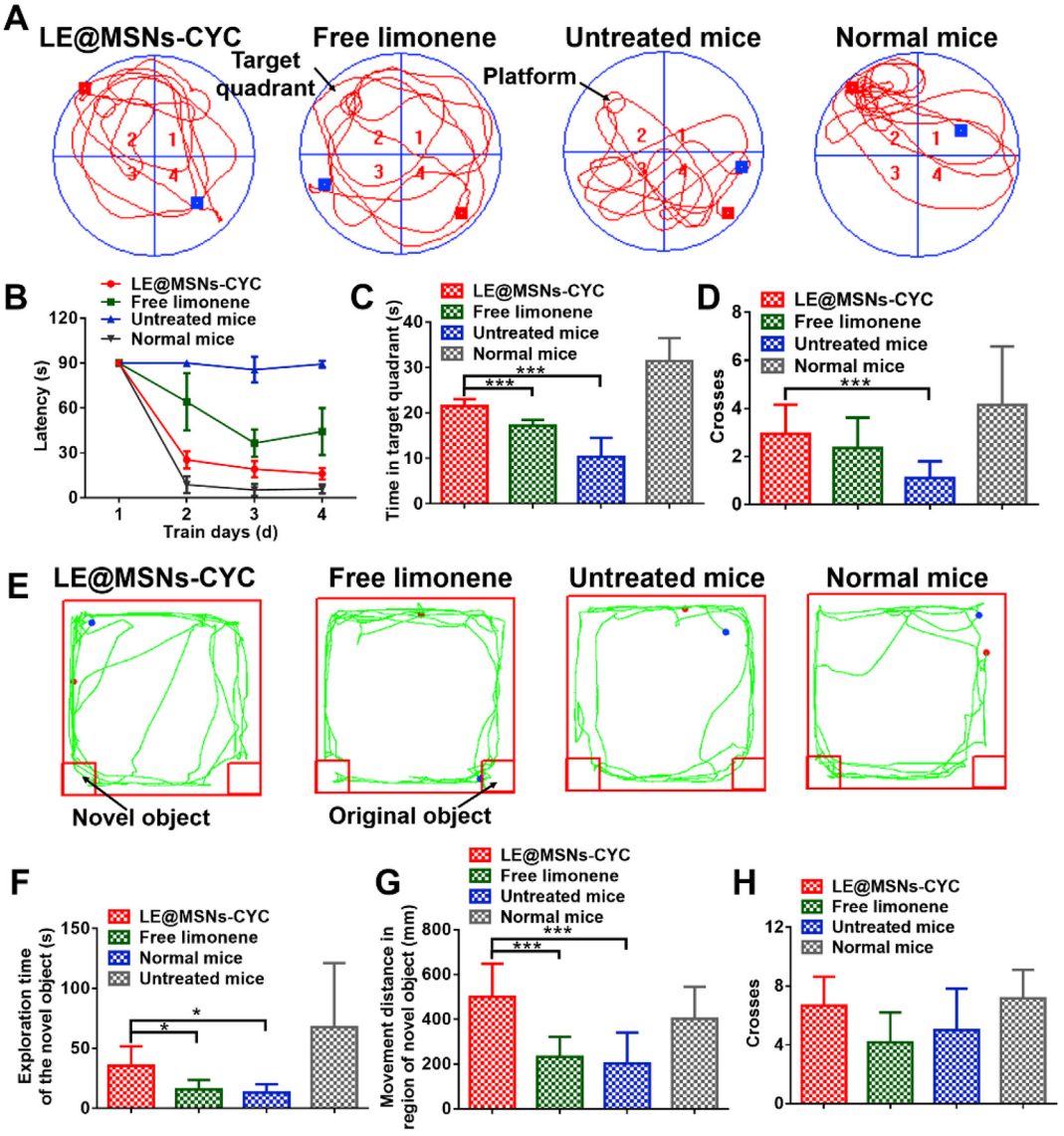

Fig. 8. (A) The swimming routes of mice in Morris water maze. (B–D) The quantified results of Fig. 8A. Mean ± SD was shown (n = 24). *P < 0.05, **P < 0.01, ***P < 0.005.(E) The movement of mice in novel object recognition tests. (F–H) The quantified results of Fig. 8E. Mean ± SD was shown (n = 6). *P < 0.05, **P < 0.01, ***P < 0.005.

percentages of movement distances in open arms. These results indicated that the simulated microgravity condition significantly impaired the movement ability of mice and increased the anxiety level of mice. Compared with free limonene treated mice and untreated mice, the exercise capacity of LE@MSNs-CYC treated mice was significantly improved, and their anxiety levels were significantly reduced.

The light-dark transition test was performed in a device that consisted of a bright box and a dark box. Mice prefer a dark environment to a strong light environment. The exploratory habits of mice prompted them to explore the light box. However, the stimulation of bright light in the open box inhibited the exploratory activities of mice.

When the anxiety level of mice decreased, their exploratory activity increased. Therefore, the anxiety level of mice can be evaluated by recording and quantifying the movements of mice in the light box and dark box [56,57]. The movements of mice were recorded in Fig. 6E. The quantified results were shown in Fig. 6F-H. Compared with the normal mice, the movement distances in light box, percentage of movement distances in light box, and the number of entries in light box of untreated mice were significantly reduced, which were consistent with the results of the elevated plus-maze tests. Compared with the mice treated with free limonene and untreated mice, the LE@MSNs-CYC treated mice moved more in the open box. These results demonstrated that the simulated microgravity condition significantly induced anxiety in mice and LE@MSNs-CYC could minimize this level of anxiety, which were consistent with the results of the elevated plus-maze tests.

The HPA axis is an important part of the neuroendocrine system, which participates in the control of stress response and regulates many physiological activities [58–60]. In particular, the HPA axis is closely related to anxiety [61,62]. Simply put, the stress response in anxiety states stimulates the HPA axis, which in turn promotes the secretion of hormones such as corticosterone, cortisol, and ATCH. The increased secretion of these hormones will further aggravate anxiety symptoms in mice [63–65]. As shown in Fig. 7A-C, the simulated microgravity condition significantly increased the secretions of corticosterone, cortisol, and ATCH in the serum of mice. But the levels of these hormones declined significantly when the mice were treated by LE@MSNs-CYC. These results indicated the anti-anxiety effect of LE@MSNs-CYC at hormone levels. GABA is an inhibitory neurotransmitter and is closely related to anxiety [66,67]. The contents of GABA in the brain of mice were measured by LC-MS. As shown in Fig. 7D, the GABA contents in

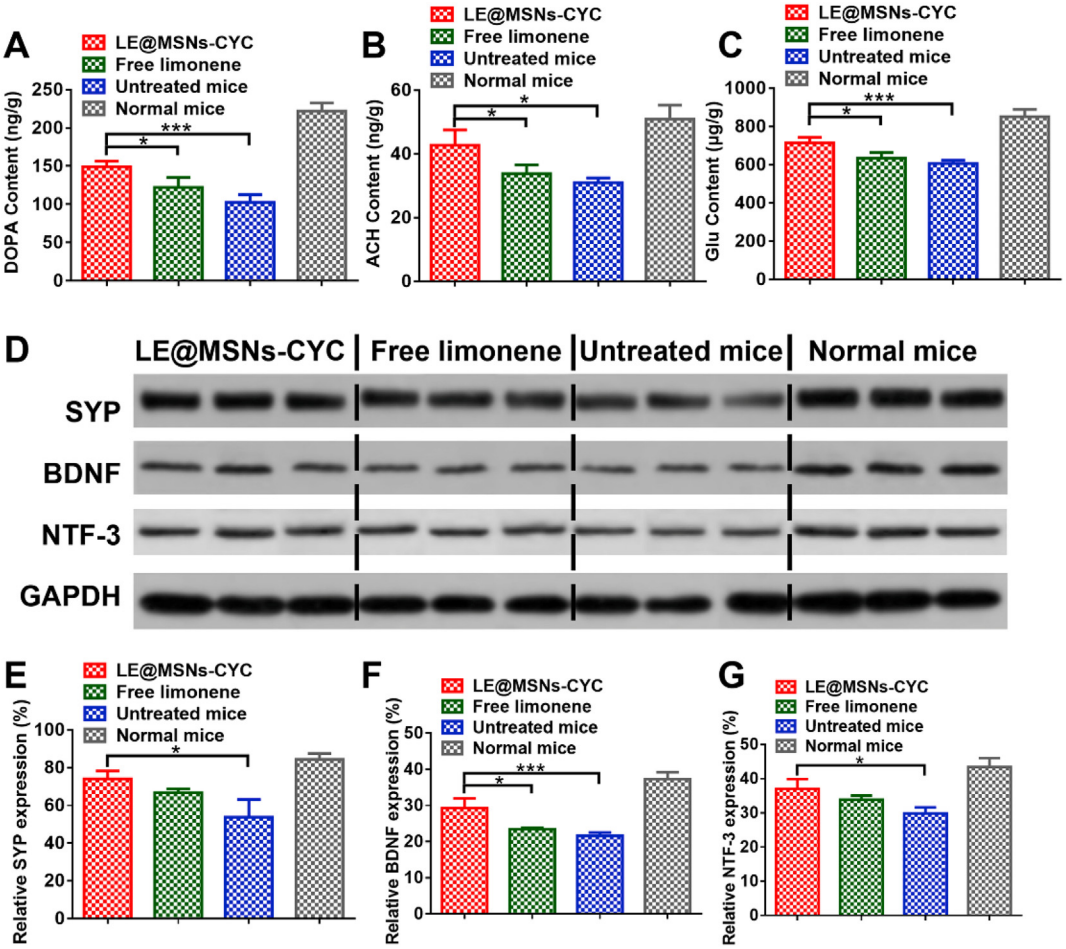

Fig. 9. (A–C) The contents of (A) DOPA, (B) ACH, and (C) Glu in the brain of mice. (D) western blot of SYP, BDNF, and NTF-3 in the brain of mice. (E–G) The quantified results of Fig. 9D. Mean ± SD was shown (n = 3). *P < 0.05, **P < 0.01, ***P < 0.005.

the brain of mice decreased significantly after cultured at the simulated microgravity condition. But, compared with free limonene, the contents of GABA in the brain of mice increased significantly after treated with LE@MSNs-CYC. This might be one of the molecular mechanisms of the anti-anxiety effects of LE@MSNs-CYC.

HPA axis is also closely related to immunity. In short, the HPA axis is stimulated to promote the secretion of corticosterone, cortisol, and ATCH under stress, which leads to the impairment of immune function. IL-1β and IL-6 are key cytokines related to immune function. As shown in Fig. 7E and F, both the contents of IL-1β and IL-6 in peritoneal macrophages were significantly increased after cultured at the simulated microgravity condition. Besides, compared with free limonene, both the contents of IL-1β and IL-6 were reduced after treated with LE@MSNs-CYC. These results indicated that the simulated microgravity condition caused the change of immune function in mice and LE@MSNs-CYC could mitigate this change. The change of immune function directly could affect health. Body weight is an important index to evaluate the health of mice. As shown in Fig. 7G and H, after 28 days, the weight of normal mice increased by 4.74%, while that of mice cultured at simulated microgravity condition decreased by 1.30%. After free limonene treatment, the weight of mice decreased by 4.39%. This might be since most of the free limonene was released into the air in a short time, resulting in extremely high concentrations of fragrance in the air. The strong aroma had side effects on mice. In contrast, the weight of mice increased by 5.08% after treated with LE@MSNs-CYC. These results indicated that the simulated microgravity condition significantly impaired the health of mice. After LE@MSNs-CYC treatment, the health of mice was significantly improved.

3.3. The effects of LE@MSNs-CYC treated wallpaper on learning and memory improvement of mice at simulated microgravity condition

Morris water maze tests are the most commonly used method to evaluate the spatial memory of animals. Simply put, mice were trained to find an underwater platform during the first four days of the tests. The time required for the mice to find the underwater platform was latency. Therefore, a short latency meant good spatial memory in the first four days. On the fifth day, the underwater platform was removed. Therefore, mice with better spatial memory were more likely to swim in the area where the original platform was located on the fifth day [68,69]. The swimming routes of mice on the fifth day were shown in Fig. 8A. As shown in Fig. 8B-D, the spatial memory ability of mice was significantly reduced after cultured at simulated microgravity conditions. But after treated with LE@MSNs-CYC, the spatial memory ability of mice recovered a lot. In contrast, the spatial memory of mice recovered poorly after treated with free limonene.

The ability of mice to remember specific things was evaluated by novel object recognition tests. In short, two identical objects were placed in two places of the box to be observed by the mice on the first day. On the second day, one of the original objects was replaced by a new one. Mice instinctively explore novel objects. Therefore, if mice remembered the original object well, they would tend to explore the new object [70,71]. The movements of mice in the boxes were shown in Fig. 8E. The exploration time of the novel object, the movement distance in the region of novel objects, and the number of crosses in the region of novel objects were quantified to more clearly analyze the exploration of mice for new objects. As shown in Fig. 8F-H, untreated

mice had significantly reduced memories of the original objects compared with normal mice. This memory ability was significantly improved after treated with LE@MSNs-CYC, while it was almost ineffective after free limonene treatment.

The memory ability of mice is closely related to the secretion of many neurotransmitters, especially DOPA, ACH, and Glu. Dopamine is a kind of monoamine neurotransmitters. The reduced contents of DOPA in the brain can lead to the loss, degeneration, or death of neurons, which further impairs learning and memory [72,73]. ACH is choline neurotransmitters. They play an important role in regulating attention, memory, and response ability [74,75]. Glu is a kind of amino acid neurotransmitters. It is the main excitatory nerve conduction medium in the brain. Besides, Glu plays an important role in learning and memory, neuronal plasticity, and brain development [76,77]. Therefore, the contents of DOPA, ACH, and Glu in the brain were measured by LC-MS. As shown in Fig. 9A-C, the simulated microgravity condition significantly reduced the contents of these three kinds of neurotransmitters in the brain. The content of neurotransmitters did not increase significantly after free limonene treatment. By contrast, treatment with LE@MSNs-CYC significantly increased the content of these neurotransmitters in the brain.

The expressions of many proteins are closely related to learning and memory function. SYP is a vesicle adsorption protein closely related to the structure and function of synapses. It is involved in the release of neurotransmitters including monoamine, choline, and amino acid. Therefore, the expression of SYP affects learning and memory [78,79]. BDNF regulates the growth of synapses, dendrites, and axons, which in turn promotes learning and memory [80,81]. NTF-3 was a kind of neurotrophic factors and closely related to learning and memory [82,83]. The contents of SYP, BDNF, and NTF-3 were measured by Western blot. Fig. 9D showed the Western blot of SYP, BNDF and NTF-3. The quantified results of Fig. 9D were shown in Fig. 9E-F. The contents of SYP, BDNF, and NTF-3 in the brain were significantly reduced after the mice were cultured at simulated microgravity conditions. Free limonene slightly increased the expression of these three proteins. In contrast, the effects of LE@MSNs-CYC on the three proteins were obvious.

4. Conclusion

In conclusion, reactive mesoporous silica nanoparticles were prepared to encapsulate limonene and the fragrance loaded nanoparticles were named LE@MSNs-CYC. LE@MSNs-CYC could chemically react with the wallpaper, so it could firmly adhere to the wallpaper. The tails of mice were suspended to simulate a microgravity environment and the ground glasses were used to isolate mice from the outside world. Compared with free limonene, LE@MSNs-CYC had better effects on anti-anxiety and improving learning and memory. Besides, LE@MSNs-CYC could also regulate the immune function of mice that cultured at the simulated microgravity condition and protected the health of mice. Therefore, LE@MSNs-CYC had the potential of aromatherapy for astronauts.

CRediT authorship contribution statement

Zhiguo Lu: Conceptualization, Methodology, Investigation, Writing - original draft. **Jianze Wang:** Investigation, Formal analysis. **Lina Qu:** Data curation, Investigation. **Guanghan Kan:** Data curation. **Tianlu Zhang:** Validation. **Jie Shen:** Investigation. **Yan Li:** Data curation. **Jun Yang:** Data curation. **Yunwei Niu:** Validation. **Zuobing Xiao:** Resources. **Yinghui Li:** Resources, Writing - review & editing, Supervision, Project administration. **Xin Zhang:** Resources, Writing - review & editing, Supervision, Project administration, Funding acquisition.

Declaration of competing interest

The authors declare that they have no known competing financial interests or personal relationships that could have appeared to influence the work reported in this paper.

Acknowledgements

This work was financially supported by the National High Technology Research and Development Program (2016YFA0200303), the Beijing Natural Science Foundation (L172046,2192057), the National Natural Science Foundation of China (31771095, 21875254 and 21905283).

References

[1] M.L. Zhou, H.C. Hu, S.H. Xu, Microgravity simulator based on air levitation for astronauts EVA operation training, Appl. Mech. Mater. 577 (2014) 443–446.
[2] M.P. Nagaraja, D. Risin, The current state of bone loss research: data from spaceflight and microgravity simulators, J. Cell. Biochem. 114 (2013).
[3] J. Ferin, G. Oberdörster, Polymer degradation and ultrafine particles: potential inhalation hazards for astronauts, Acta Astronaut. 27 (1992) 257–259.
[4] Tachibana Koji, Tachibana Shoichi, Inoue Natsuhiko, From outer space to Earth—the social significance of isolated and confined environment research in human space exploration, Acta Astronaut. 140 (2017) 273–283.
[5] T. Mano, N. Nishimura, S. Iwase, Sympathetic neural influence on bone metabolism in microgravity (Review), Acta Physiol. Hung. 97 (4) (2010) 354–361.
[6] E. Blaber, H. Marcal, B.P. Burns, Bioastronautics: the influence of microgravity on, Astronaut Health, Astrobiology 10 (5) (2010) 463–473.
[7] E. Albi, M. Kruger, R. Hemmersbach, A. Lazzarini, S. Cataldi, M. Codini, T. Beccari, F.S. Ambesiimpiombato, F. Curcio, Impact of gravity on thyroid cells, Int. J. Mol. Sci. 18 (5) (2017) 972–985.
[8] A. Giuliani, S. Mazzoni, A. Ruggiu, B. Canciani, R. Cancedda, S. Tavella, High-resolution X-ray tomography: a 3D exploration into the skeletal architecture in mouse models submitted to microgravity constraints, Front. Physiol. 9 (181) (2018) 1–7.
[9] B. Yulug, G. Erkol, E. Kilic, An interesting link between microgravity and psychiatric diseases, J. Neuropsychiatry 22 (4) (2010) 451-451.
[10] H. Qin, Y. Bai, B. Wu, J. Wang, X. Liu, Progress of study on emotion in manned spaceflight, Space Med. Med. Eng. 25 (4) (2012) 302–306.
[11] H.S. Cooper, The loneliness of the long-duration astronaut, Air Space Smithsonian 11 (2) (1996) 37–45.
[12] D. Li, X.M. Liu, W.U. Li-Sha, S.J. Yang, Q. Wang, Effect of aerospace weightlessness on cognitive functions and the relative dialectical analysis of Chinese medicine, Chin. J. Integr. Tradit. West. Med. 34 (3) (2014) 355–358.
[13] L.K. Barger, K.P. Wright, T.M. Burke, E.D. Chinoy, J.M. Ronda, S.W. Lockley, C.A. Czeisler, Sleep and cognitive function of crewmembers and mission controllers working 24-h shifts during a simulated 105-day spaceflight mission, Acta Astronaut. 93 (2014) 230–242.
[14] H. Hashizume, T. Horibe, A. Ohshima, T. Ito, H. Yagi, M. Takigawa, Anxiety accelerates T-helper 2-tilted immune responses in patients with atopic dermatitis, Br. J. Dermatol. 152 (6) (2005) 1161–1164.
[15] L. Arranz, N. Guayerbas, L. Siboni, D.L.F. Mónica, Effect of acupuncture treatment on the immune function impairment found in anxious women, Am. J. Chin. Med. 35 (2007) 35–51 01.
[16] H. Qin, Q. Pei, B. Wu, L. Tian, J. Wang, L. Fang, Effects of music relaxation on personnel's stress and emotion, Space Med. Med. Eng. 30 (2017) 176–179.
[17] M. Yamaguchi, N. Hanawa, K. Hamazaki, K. Sato, K. Nakano, Evaluation of the acute sedative effect of fragrances based on a biochemical marker, J. Essent. Oil Res. 19 (5) (2007) 470–476.
[18] C. Dobetsberger, G. Buchbauer, Actions of essential oils on the central nervous system: an updated review, Flavour Fragrance J. 26 (5) (2011) 300–316.
[19] Z. Lu, T. Zhang, X. Wang, J. Wang, J. Shen, Z. Xiao, L. Chen, X. Zhang, Zwitterionic polymer-based nanoparticles encapsulated with linalool for regulating central nervous system, ACS Biomater. Sci. Eng. 6 (1) (2020) 442–449.
[20] G. Buchbauer, L. Jirovetz, W. Jager, C. Plank, H. Dietrich, Fragrance compounds and essential oils with sedative effects upon inhalation, J. Pharmaceut. Sci. 82 (6) (1993) 660–664.
[21] A.M. Borda, D.G. Clark, D.J. Huber, B.A. Welt, T.A. Nell, Effects of ethylene on volatile emission and fragrance in cut roses: the relationship between fragrance and vase life, Postharvest Biol. Technol. 59 (3) (2011) 245–252.
[22] D. Berthier, I. Schmidt, W. Fieber, C. Schatz, A. Furrer, K. Wong, S. Lecommandoux, Controlled release of volatile fragrance molecules from PEO-b-PPO-b-PEO block copolymer micelles in Ethanol−Water mixtures, Langmuir 26 (11) (2010) 7953–7961.
[23] I. Hofmeister, K. Landfester, A. Taden, pH-Sensitive nanocapsules with barrier properties: fragrance encapsulation and controlled release, Macromolecules 47 (16) (2014) 5768–5773.
[24] B. Indradas, C. Hansen, M. Palmer, G.B. Womack, Autoxidation as a trigger for the slow release of volatile perfumery chemicals, Flavour Fragrance J. 29 (5) (2014) 313–323.
[25] R. Lopes, M.M. Gaspar, J.D. Pereira, C. Eleuterio, M. Carvalheiro, A.J. Almeida, M. Cruz, Liposomes versus lipid nanoparticles: comparative study of lipid-based systems as oryzalin carriers for the treatment of leishmaniasis, J. Biomed. Nanotechnol. 10 (12) (2014) 3647–3657.

[26] Hussain Saxena, Polymeric mixed micelles for delivery of curcumin to multidrug resistant ovarian cancer, J. Biomed. Nanotechnol. 9 (7) (2013) 1146–1154.
[27] D.J. Fu, Y. Jin, M.Q. Xie, Y.J. Ye, D.D. Qin, K.Y. Lou, Y.Z. Chen, Preparation and characterization of mPEG grafted chitosan micelles as 5-fluorouracil carriers for effective anti-tumor activity, Chin. Chem. Lett. 25 (11) (2014) 1435–1440.
[28] L. Xu, W. Qiu, W. Liu, C. Zhang, M. Zou, Y. Sun, X. Zhang, PLA–PEG micelles loaded with a classic vasodilator for oxidative cataract prevention, ACS Biomater. Sci. Eng. 5 (2) (2019) 407–412.
[29] Z. Guo, S. Li, Z. Liu, W. Xue, Tumor-Penetrating Peptide-Functionalized Redox-Responsive Hyperbranched Poly(amido Amine) Delivering siRNA for Lung Cancer Therapy, ACS Biomaterials Science & Engineering, 2018.
[30] J. Zhang, J. Cui, Y. Deng, Z. Jiang, W.M. Saltzman, Multifunctional poly(amine-co-ester-co-orthoester) for efficient and safe gene delivery, ACS Biomater. Sci. Eng. 2 (11) (2016) 2080–2089.
[31] H.J. Yan, D.C. Zhu, Z.X. Zhou, X. Liu, Y. Piao, Z. Zhang, X.R. Liu, J.B. Tang, Y.Q. Shen, Facile synthesis of semi-library of low charge density cationic polyesters from poly(alkylene maleate)s for efficient local gene delivery, Biomaterials 178 (2018) 559–569.
[32] D. Li, X. Feng, L. Chen, J. Ding, X. Chen, One-step synthesis of targeted acid-labile polysaccharide prodrug for efficiently intracellular drug delivery, ACS Biomater. Sci. Eng. 4 (2) (2018) 539–546.
[33] M. Ni, W. Zeng, X. Xie, Z. Chen, H. Wu, C. Yu, B. Li, Intracellular enzyme-activatable prodrug for real-time monitoring of chlorambucil delivery and imaging, Chin. Chem. Lett. 28 (6) (2017) 1345–1351.
[34] Q. Zhou, S.Q. Shao, J.Q. Wang, C.H. Xu, J.J. Xiang, Y. Piao, Z.X. Zhou, Q.S. Yu, J.B. Tang, X.R. Liu, Z.H. Gan, R. Mo, Z. Gu, Y.Q. Shen, Enzyme-activatable polymer-drug conjugate augments tumour penetration and treatment efficacy, Nat. Nanotechnol. 14 (8) (2019) 799–+.
[35] J.Q. Wang, S.Q. Hu, W.W. Mao, J.J. Xiang, Z.X. Zhou, X.R. Liu, J.B. Tang, Y.Q. Shen, Assemblies of peptide-cytotoxin conjugates for tumor-homing chemotherapy (vol 29, 1807446, 2019), Adv. Funct. Mater. 29 (32) (2019).
[36] Q. Meng, H. Hu, L. Zhou, Y. Zhang, B. Yu, Y. Shen, H. Cong, Logical design and application of prodrug platforms, Polym. Chem. 10 (3) (2019) 306–324.
[37] Y. Wang, Y. Yan, J. Cui, L. Hostarigau, J.K. Heath, E.C. Nice, F. Caruso, Encapsulation of water-insoluble drugs in polymer capsules prepared using mesoporous silica templates for intracellular drug delivery, Adv. Mater. 22 (38) (2010) 4293–4297.
[38] S. Chen, X. Hao, X. Liang, Q. Zhang, C. Zhang, G. Zhou, S. Shen, G. Jia, J.Z. Zhang, Inorganic nanomaterials as carriers for drug delivery, J. Biomed. Nanotechnol. 12 (1) (2016) 1.
[39] Z. Mohamadnia, E. Ahmadi, M. Ghasemnejad, S. Hashemikia, A. Doustgani, Surface modification of mesoporous nanosilica with [3-(2-Aminoethylamino) propyl] trimethoxysilane and its application in drug delivery, Int. J. Nanosci. Nanotechnol. 11 (3) (2015) 167–177.
[40] S.K. Parida, S. Dash, S. Patel, B.K. Mishra, Adsorption of organic molecules on silica surface, Adv Colloid Interfac 121 (1–3) (2006) 77–110.
[41] Y. Zhang, Q. Wang, H. Chen, X. Liu, K. Lv, T. Wang, Y. Wang, G. Ji, H. Cao, G. Kan, Y. Li, L. Qu, Involvement of cholinergic dysfunction and oxidative damage in the effects of simulated weightlessness on learning and memory in rats, BioMed Res. Int. 2018 (2018) 2547532.
[42] A. Szegedi, M. Popova, I. Goshev, J. Mihaly, Effect of amine functionalization of spherical MCM-41 and SBA-15 on controlled drug release, J. Solid State Chem. 184 (5) (2011) 1201–1207.
[43] K. Abdollahi, F. Yazdani, R. Panahi, Covalent immobilization of tyrosinase onto cyanuric chloride crosslinked amine-functionalized superparamagnetic nanoparticles: synthesis and characterization of the recyclable nanobiocatalyst, Int. J. Biol. Macromol. 94 (2017) 396–405.
[44] Z.G. Lu, T.L. Zhang, J. Yang, J.Z. Wang, J. Shen, X.Y. Wang, Z.B. Xiao, Y.W. Niu, G.Y. Liu, X. Zhang, Effect of mesoporous silica nanoparticles-based nano-fragrance on the central nervous system, Eng. Life Sci. (2020).
[45] J. Shen, Z.G. Lu, T.L. Zhang, Z.B. Xiao, J. Hu, Y.W. Niu, D. Yu, Y.P. Wei, G.Y. Liu, X. Zhang, Effects of wallpaper with the ability of photo-activated releasing fragrance on central nervous system, J. Biomed. Nanotechnol. 14 (9) (2018) 1556–1567.
[46] T. Wang, H. Chen, K. Lv, G. Ji, Y. Zhang, Y. Wang, Y. Li, L. Qu, iTRAQ-based proteomics analysis of hippocampus in spatial memory deficiency rats induced by simulated microgravity, J Proteomics 160 (2017) 64–73.
[47] Z.G. Lu, Y.C. Zheng, T.L. Zhang, J. Shen, Z.B. Xiao, J. Hu, Y.W. Niu, D. Yu, X. Zhang, Effects of photo-activated nanomicelles loaded with fragrance on central nervous system, J. Biomed. Nanotechnol. 14 (10) (2018) 1675–1687.
[48] C.H. Bueno, H. Zangrossi, M.B. Viana, The inactivation of the basolateral nucleus of the rat arnygdala has an anxiolytic effect in the elevated T-maze and light/dark transition tests, Braz. J. Med. Biol. Res. 38 (11) (2005) 1697–1701.
[49] L. Rajagopal, B.W. Massey, M. Huang, Y. Oyamada, H.Y. Meltzer, The novel object recognition test in rodents in relation to cognitive impairment in schizophrenia, Curr. Pharmaceut. Des. 20 (31) (2014) 5104–5114.
[50] R.Y. Liu, J. Yang, L.Y. Liu, Z.G. Lu, Z.Y. Shi, W.H. Ji, J. Shen, X. Zhang, An "Amyloid-beta cleaner" for the treatment of alzheimer's disease by normalizing microglial dysfunction, Adv. Sci. 7 (2) (2020).
[51] Z. Lu, T. Zhang, J. Shen, Z. Xiao, J. Hu, Y. Niu, D. Yu, L. Chen, X. Zhang, Effects of fragrance-loaded mesoporous silica nanocolumns on central nervous system, J. Biomed. Nanotechnol. 14 (9) (2018) 1578–1589.
[52] R.K. Kankala, C.G. Liu, D.Y. Yang, S.B. Wang, A.Z. Chen, Ultrasmall platinum nanoparticles enable deep tumor penetration and synergistic therapeutic abilities through free radical species-assisted catalysis to combat cancer multidrug resistance, Chem. Eng. J. 383 (2020).
[53] R.K. Kankala, C.G. Liu, A.Z. Chen, S.B. Wang, P.Y. Xu, L.K. Mende, C.L. Liu, C.H. Lee, Y.F. Hu, Overcoming multidrug resistance through the synergistic effects of hierarchical pH-sensitive, ROS-generating nanoreactors, ACS Biomater. Sci. Eng. 3 (10) (2017) 2431–2442.
[54] S. Darbra, M. Pallares, Effects of early postnatal allopregnanolone administration on elevated plus maze anxiety scores in adult male wistar rats, Neuropsychobiology 65 (1) (2012) 20–27.
[55] S. Pellow, P. Chopin, S.E. File, M. Briley, Validation of open - closed arm entries in an elevated plus-maze as a measure of anxiety in the rat, J. Neurosci. Methods 14 (3) (1985) 149–167.
[56] T. Shimada, K. Matsumoto, M. Osanai, H. Matsuda, K. Terasawa, H. Watanabe, The modified light/dark transition test in mice - evaluation of classic and putative anxiolytic and anxiogenic drugs, Gen. Pharmacol. 26 (1) (1995) 205–210.
[57] A. Bilkei-Gorzo, I. Gyertyan, G. Levay, mCPP-induced anxiety in the light-dark box in rats - a new method for screening anxiolytic activity, Psychopharmacology 136 (3) (1998) 291–298.
[58] L. Ayer, K. Greaves-Lord, R.R. Althoff, J.J. Hudziak, G.C. Dieleman, F.C. Verhulst, V.D.E. Jan, Blunted HPA axis response to stress is related to a persistent Dysregulation Profile in youth, Biol. Psychol. 93 (3) (2013) 343–351.
[59] L.M. Holsen, K. Lancaster, A. Klibanski, S. Whitfield-Gabrieli, S. Cherkerzian, S. Buka, J.M. Goldstein, HPA-axis hormone modulation of stress response circuitry activity in women with remitted major depression, Neuroscience 250 (2013) 733–742.
[60] J.S. Jackson, K.M. Knight, J.A. Rafferty, Race and unhealthy behaviors: chronic stress, the HPA Axis, and physical and mental health disparities over the life course, Am. J. Publ. Health 100 (5) (2010) 933–939.
[61] V.L. Kallen, J.H.M. Tulen, E.M.W.J. Utens, P.D.A. Treffers, F.H.D. Jong, R.F. Ferdinand, Associations between HPA axis functioning and level of anxiety in children and adolescents with an anxiety disorder, Depress. Anxiety 25 (2) (2010) 131–141.
[62] P. Verma, K.G.C. Hellemans, F.Y. Choi, W. Yu, J. Weinberg, Circadian phase and sex effects on depressive/anxiety-like behaviors and HPA axis responses to acute stress, Physiol. Behav. 99 (3) (2010) 285 0.
[63] E. Ducat, B. Ray, G. Bart, Y. Umemura, J. Varon, A. Ho, M.J. Kreek, Mu-opioid receptor A118G polymorphism in healthy volunteers affects hypothalamic–pituitary–adrenal axis adrenocorticotropic hormone stress response to metyrapone, Addiction Biol. 18 (2) (2013) 325–331.
[64] A.S. Koe, M.R. Salzberg, M.J. Morris, T.J. O'Brien, N.C. Jones, Early life maternal separation stress augmentation of limbic epileptogenesis: the role of corticosterone and HPA axis programming, Psychoneuroendocrinology 42 (2014) 124–133.
[65] B. Adinoff, K. Junghanns, F. Kiefer, S. Krishnansarin, Suppression of the HPA Axis stress-response: implications for relapse, Alcohol Clin. Exp. Res. 29 (7) (2005) 1351–1355.
[66] H. Möhler, The GABA system in anxiety and depression and its therapeutic potential, Neuropharmacology 62 (1) (2012) 42–53.
[67] A. Pilc, G. Nowak, GABAergic hypotheses of anxiety and depression: focus on GABA-B receptors, Drugs Today 41 (11) (2005) 755.
[68] C.V. Vorhees, M.T. Williams, Morris water maze: procedures for assessing spatial and related forms of learning and memory, Nat. Protoc. 1 (2) (2006) 848–858.
[69] C.D. Barnhart, D.R. Yang, P.J. Lein, Using the Morris water maze to assess spatial learning and memory in weanling mice, PloS One 10 (4) (2015).
[70] P.K. Chang, L. Yu, J.C. Chen, Dopamine D3 receptor blockade rescues hyper-dopamine activity-induced deficit in novel object recognition memory, Neuropharmacology 133 (2018) 216–223.
[71] N.M. Neugebauer, M. Miyauchi, T. Sato, J. Tadano, H. Akal, H. Ardehali, H.Y. Meltzer, Hippocampal GABA(A) antagonism reverses the novel object recognition deficit in sub-chronic phencyclidine-treated rats, Behav. Brain Res. 342 (2018) 11–18.
[72] A. Nobili, E.C. Latagliata, M.T. Viscomi, V. Cavallucci, D. Cutuli, G. Giacovazzo, P. Krashia, F. Rizzo, R. Marino, M. Federici, Dopamine neuronal loss contributes to memory and reward dysfunction in a model of Alzheimer's disease, Nat. Commun. 8 (1) (2017) 14727–14740.
[73] P.S. Goldman-Rakic, The cortical dopamine system: role in memory and cognition, Adv. Pharmacol. 42 (1998) 707–711.
[74] J. Winkler, S.T. Suhr, F.H. Gage, L.J. Thal, L.J. Fisher, Essential role of neocortical acetylcholine in spatial memory, Nature 375 (6531) (1995) 484–487.
[75] J. Micheau, A. Marighetto, Acetylcholine and memory: a long, complex and chaotic but still living relationship, Behav. Brain Res. 221 (2) (2011) 429 0.
[76] G.L. Collingridge, W. Singer, Excitatory amino acid receptors and synaptic plasticity, Trends Pharmacol. Sci. 11 (7) (1990) 290–296.
[77] E.O. Álvarez, M.B. Ruarte, Glutamic acid and histamine-sensitive neurons in the ventral hippocampus and the basolateral amygdala of the rat: functional interaction on memory and learning processes, Behav. Brain Res. 152 (2) (2004) 219 0.
[78] K.M. Frick, S.M. Fernandez, Enrichment enhances spatial memory and increases synaptophysin levels in aged female mice, Neurobiol. Aging 24 (4) (2003) 626 0.
[79] Q. Li, X.L. Zhu, A.P. Jin, X.Y. Liu, Y.X. Zhao, Inhibition of synaptophysin ubiquitination may improve the intelligent drop due to high glucose and hypoxia, Int. J. Clin. Exp. Med. 7 (12) (2014) 5021–5030.
[80] M.F. Egan, M. Kojima, J.H. Callicott, T.E. Goldberg, B.S. Kolachana, A. Bertolino, E. Zaitsev, B. Gold, D. Goldman, M. Dean, The BDNF val66met polymorphism affects activity-dependent secretion of BDNF and human memory and hippocampal function, Cell 112 (2) (2003) 257–269.
[81] J.H. Medina, BDNF and memory formation and storage, Neuroscientist A Review Journal Bringing Neurobiology Neurology & Psychiatry 14 (2) (2008) 147.
[82] L.K. Ferrarelli, Repurposing statins for Alzheimer's disease, Sci. Signal. 8 (389) (2015).
[83] H.F. Farhadi, M.S. Javad, P. Kevin, S.J. Morris, N.G. Seidah, R.A. Murphy, Neurotrophin-3 sorts to the constitutive secretory pathway of hippocampal neurons and is diverted to the regulated secretory pathway by coexpression with brain-derived neurotrophic factor, J. Neurosci. 20 (11) (2000) 4059–4068.